

Optimising gravitational waves follow-up using galaxies stellar mass

J. -G. Ducoin¹, D. Corre¹, N. Leroy¹, E. Le Floch²

¹*LAL, Univ Paris-Sud, CNRS/IN2P3, Orsay, France*

²*IRFU, CEA, Univ Paris-Saclay, Gif-sur-Yvette, France*

Accepted XXX. Received YYY; in original form ZZZ

ABSTRACT

We present a new strategy to optimise the electromagnetic follow-up of gravitational wave triggers. This method is based on the widely used galaxy targeting approach where we add the stellar mass of galaxies in order to prioritise the more massive galaxies. We crossmatched the GLADE galaxy catalog with the AllWISE catalog up to 400Mpc with an efficiency of $\sim 93\%$, and derived stellar masses using a stellar-to-mass ratio using the WISE1 band luminosity. We developed a new grade to rank galaxies combining their 3D localisation probability associated to the gravitational wave event with the new stellar mass information. The efficiency of this new approach is illustrated with the GW170817 event, which shows that its host galaxy, NGC4993, is ranked at the first place using this new method. The catalog, named Mangrove, is publicly available and the ranking of galaxies is automatically provided through a dedicated web site for each gravitational wave event.

Key words: gravitational waves – catalogues – methods: observational

1 INTRODUCTION

Gravitational waves from binary neutron star (BNS) coalescence, in association to short gamma-ray burst, opened a new era of multi-messenger astronomy. The event of the 17th august 2017 was a real breakthrough for the multi-messenger astronomy. For the first time, an electromagnetic counterpart of a gravitational wave was observed (Abbott et al. 2017a). The association with a gamma ray burst (GRB) detected by Fermi-GBM a few seconds after the coalescence provides the first evidence of a link between BNS merger and short gamma ray burst. The huge effort of ground telescopes follow-up in association to the relative small volume of this event localisation in the sky, allowed the identification of the GW electromagnetic counterpart. The multi-wavelength observations improved our understanding of the physics of strong-gravity and put some constraints on astrophysical models related to matter during the merger and post-merger phase. A first constraint of the speed of gravitational waves and violation of Lorentz invariance has been determined from this event (Abbott et al. 2017b). Both kilonova and afterglow observations provide information about the neutron star equation of state, energy of the ejecta, merger remnant, ambient medium and so on (Abbott et al. 2018c; Hajela et al. 2019; Gill et al. 2019). Such event also provide a new independent

derivation of the Hubble Constant (Coughlin et al. 2019a). The third LIGO-Virgo run (O3) started the first of April 2019 and multi-messenger astronomy related to gravitational waves with it. With improved sensitivity of the LIGO-Virgo detectors, the year-long third observing run (O3) has already brought his share of merging binaries and promises many more of them. Therefore an intensive multi-wavelength follow-up of those events with ground and space instruments is performed all around the world. But the identification of the electromagnetic counterpart of such event is very challenging knowing the wide sky localization area provided by LIGO-Virgo (which can span more than 1000 deg^2) and require complex observation strategies.

Many efforts were done recently to optimise the observations for these large sky areas (Ghosh et al. 2016a; Coughlin et al. 2019b). For large field of view (FoV) telescope the standard approach consists in observing the localisation error box provided by LIGO-Virgo (Singer & Price 2016; Veitch et al. 2015) using an optimised tiling of the sky (Coughlin et al. 2018). In such standard strategy, the scheduling of the tile observation is provided by the 2D probability distribution from LIGO-Virgo skymaps.

More recent works tried to include galaxies population to the strategy (Arcavi et al. 2017; Antolini et al. 2017; Rana & Mooley 2019). Such developments allow to use the

3D probability distribution from the LIGO-Virgo skymap (and not only the 2D probability) to produce a "galaxy weighting" rank for the tiles. It also allows to provide a scheduling of observation for narrow FoV telescopes. Indeed, with such information we can provide a list of interesting galaxies (i.e. ranked by their 3D position probability inside the LIGO-Virgo skymap) to be observed by these small FoV telescopes. To allow the use of information related to galaxies, one must rely on a galaxy catalog that is sufficiently complete compared to the interferometers sensitivity range. The current binary neutron star range is at 130 Mpc for LIGO Livingston, 110 Mpc for LIGO Hanford, and 50 Mpc for Virgo (Abbott et al. 2018a). The CLU catalog (Cook et al. 2019) for the north hemisphere contains the WISE1 luminosity information as well as spectroscopic measurement of local galaxies, however it is non publicly available. Therefore, for the purpose of our work, we rely on the publicly available GLADE galaxy catalog (Dályá et al. 2018) which is all-sky and complete up to 100Mpc, and nearly complete up to 150Mpc.

Given the large size of error boxes, the number of galaxies compatible with an event can be very large (>few thousands). In such cases, the classification using the 3D probability only is limited because it will produce similar values for a large number of galaxies. Adding galaxy properties to the ranking is a way to reduce the sample size of interesting galaxies. Among the various galaxies properties that could influence the rate of BNS merger, such as star formation rate (SFR), stellar mass and metallicity, several works pointed out a significant dependence to the stellar mass (Artale et al. 2019; Toffano et al. 2019; Mapelli et al. 2018). Furthermore, short GRB host galaxies are known to be associated to BNS merger since GW170817, and are found in massive galaxies. The short GRB host galaxies are more massive than the long GRBs host galaxies, pointing to the importance of the stellar mass in determining the rate of short GRBs (Leibler & Berger 2010; Berger 2014). So far, there has been only two identified host galaxies of BNS merger events, GW170817 and short GRB 150101B. They are both massive galaxies with low star formation rates (Xie et al. 2016; Im et al. 2017). In the light of those information we chose to focus on the stellar mass for the selection of gravitational waves host galaxy candidates.

In Section 2, we describe the general galaxy targeting approach and the new formulation we propose to include the stellar mass information. In the Section 3 we describe the crossmatch between the GLADE and AllWISE catalogs and the stellar mass estimation as well as an estimation of the completeness of the resulting Mangrove (Mass Association for GRavitational waves Observations Efficiency) catalog in terms of stellar mass. In Section 4 we test our method on the GW170817 event. In Section 5 we discuss future development of this method for wide field of view telescopes.

2 GALAXY TARGETING METHOD

In this section, we first describe the standard galaxy approach using the 3D localisation of the GW skymap, and

then we propose a new formulation of the grade used to rank galaxies in order to include the stellar mass information.

2.1 Standard approach

In case of a gravitational wave event, LIGO-Virgo rapidly releases a probability skymap based on the distance and two dimensional localisation of the event allowing to constrain the region of the sky to search for the GW electromagnetic counterpart (Singer & Price 2016). With such skymap we are able to fetch the probability density per unit of volume at a given position (Singer et al. 2016). This is used to infer the probability of a given galaxy to be the host of the merger according to its celestial position P_{pos} with the following relation:

$$P_{pos} = P_{dV} = \frac{P_{pixel}}{Pixel\ area} N_{pixel} e^{-\frac{1}{2} \left(\frac{D_{galaxy} - \mu_{pixel}}{\sigma_{pixel}} \right)^2} \quad (1)$$

Where P_{pixel} is the 2D probability included in the given pixel, N_{pixel} is the normalisation factor for the given pixel, μ_{pixel} is the mean distance value at the given pixel, σ_{pixel} is the standard deviation at the given pixel and D_{galaxy} is the luminosity distance of the galaxy fetched from the galaxy catalog. The outputs of the LIGO-Virgo localization pipelines are HEALPix (Hierarchical Equal Area isoLatitude Pixelization) all-sky images, the skymap we are dealing with is composed of pixels defined by the HEALPix (Górski et al. 2005) format.

For the selection of the galaxies, we classified as "compatible" with the skymap, a galaxy which fulfills the two following conditions:

- Its 2D position in the sky as to be in the 90% of the 2D skymap probability distribution.
- Its distance has to fall within the 3 sigma distance error localization at the given pixel of the galaxy.

With such conditions we ensure that telescopes will not point outside of the 90% skymap probability distribution. The conservative choice of 3σ on the distance constraint is motivated by the fact that galaxies with a low distance probability will be always penalised in the ranking process. Regarding the condition on the distance, we use the pixel by pixel information and not the mean distance estimation for the LIGO-Virgo candidate, as in the approach adopted by (Arcavi et al. 2017). This is more efficient because the distance estimation can be very inhomogeneous in a given skymap. The figure 1 shows the distribution pixel by pixel of the mean distance μ and the standard deviation σ inside the the 90% of the 2D skymap probability distribution for the S190425z candidate during the O3 run. This example of a BNS candidate shows that for a large portion of the skymap the μ and σ at a given pixel are far away from the mean distance evaluation for the whole skymap (155 ± 45 Mpc in this case). Using pixel by pixel information prevents to dismiss compatible galaxies or select incompatible ones. One of the main advantage of the galaxy targeting is to reduce the amount of observations necessary to cover a given skymap. The figure 2 shows the result of the galaxy targeting for GW170817 with a standard field of view of 20 arcmin. A large part of the skymap is not worth observing because it does not contain any compatible galaxies. A total

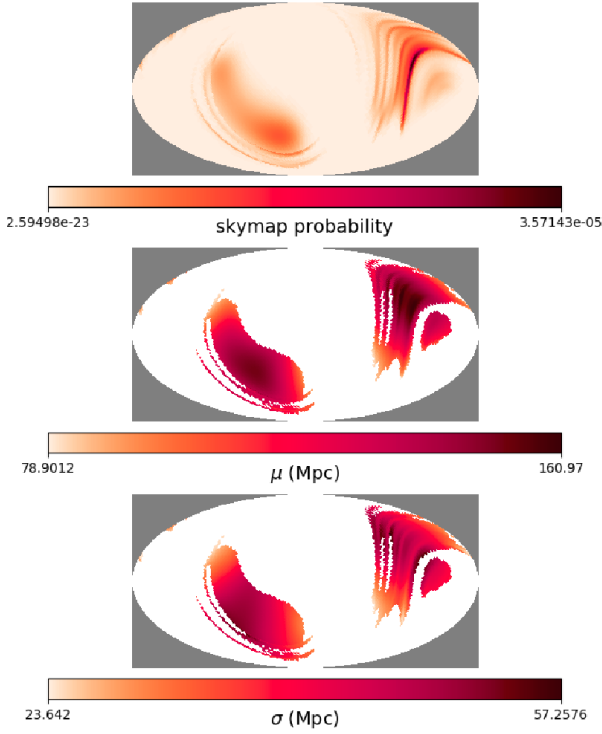


Figure 1. The top plot show the probability distribution for the BNS candidate S190425z of O3. The middle and bottom plot are respectively the mean distance and its standard deviation distributions for the pixels inside the the 90% of the 2D skymap probability distribution

of 44 pointing are needed to observe all galaxies compatible with the 90% skymap whereas it would have required 144 tiles to cover the entire 90% skymap, which results on significant gain of observational time allocation and revisits.

In such a standard strategy only the 3D position of the galaxy is used, and a more advanced strategy is to include physical properties of the galaxies such as the stellar mass as the host galaxy of BNS counterparts are likely to be found in massive galaxies.

2.2 Grade reformulation with stellar mass

In this section, we describe how to take into account the stellar mass information in the galaxy ranking process, in order to prioritize massive galaxies. We introduce a new term P_{mass} defined as:

$$P_{mass} = \frac{M_{*,galaxy}}{\sum M_{*,galaxy}} \quad (2)$$

where $M_{*,galaxy}$ is the stellar mass of a given galaxy and the sum is over all of the galaxies compatibles with a given skymap (see 2 for the definition). This We first combine this term to the standard grade defined in equation (1) for each galaxy computing the product as:

$$P_{tot} = P_{pos} \times P_{mass} \quad (3)$$

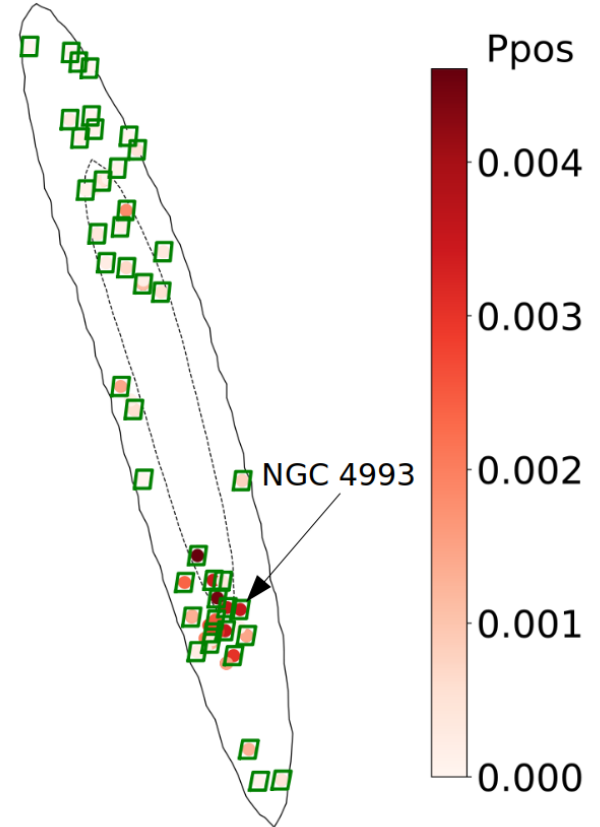


Figure 2. Skymap of GW170817. The dashed and the solid line enclose respectively the 50% and the 90% of the skymap. The green squares represent the pointing of a telescope with a field of view of 20'. The red color scale show the grade of the galaxies according to (3). The black arrow show the position of the GW host galaxy, NGC 4993.

The equation (3) is proposed to fit with (Arcavi et al. 2017) expression to allow a direct comparison of the results (see Section 4), but the drawback of this expression with a simple product is that galaxies for which no stellar mass is available are simply not considered. In order to keep galaxies without stellar mass information, and still use their 3D localisation probability, P_{pos} from equation (1), we propose to redefine the grade defined in equation (3) as:

$$P_{tot} = P_{pos} (1 + \alpha \beta P_{mass}) \quad (4)$$

where α and β are positive real parameters. With such definition, P_{mass} is set to 0 when the stellar mass information is not available to fall back on P_{pos} . The parameter α is defined such that the two terms in equation (4) contribute equally to the total grade, P_{tot} :

$$\frac{\sum P_{pos}}{N} = \frac{\sum P_{pos} \alpha P_{mass}}{N} \quad (5)$$

$$\Rightarrow \alpha = \frac{\sum P_{pos}}{\sum P_{pos} P_{mass}} \quad (6)$$

where N is the total number of galaxies compatible for a given skymap having a determined stellar mass, and the

sum is also over all galaxies compatible for a given skymap having a determined stellar mass. The parameter β is used to weight the importance of P_{mass} in the total grade, it is skymap independent. Ideally, β should be fitted on a statistically significant sample of gravitational wave host galaxies, but as only one event has been detected so far, we simply chose to put β equal to one.

Previous works (Arcavi et al. (2017); Salafia et al. (2017)) chose to include an other factor of the grade which describe the likelihood to detect the counterpart according to limiting magnitude of the observing telescope and the expected magnitude of the source. Such factor can be added to the expression (3) and (4) if needed. We choose not to develop such strategy because first the limiting magnitude of a telescope can vary a lot between two observations (seeing, horizon...) and secondly only one detection of gravitational wave electromagnetic counterpart has been achieved at the moment, so only one one set of data describing the expected kilonova lightcurve is available and assuming a standard lightcurve on a single object could be risky.

3 ADDING STELLAR MASS TO GLADE CATALOG

In this section we aim at adding the stellar mass for the GLADE galaxy catalog. In the first part, we describe how to derive the stellar mass from the WISE1 band luminosity. In the second part we study the completeness of the Mangrove catalog resulting from the crossmatch between GLADE and AllWISE catalogs.

3.1 WISE1 band as a prob of stellar mass

We rely on the GLADE galaxy catalog to retrieve the galaxies compatible for a given GW skymap. In this catalog, the B, J, H and K band magnitudes are provided for some of the galaxies. Previous work (Arcavi et al. 2017) used the B band magnitude included in the GLADE catalog as an indicator of the stellar mass. However, the B band is sensitive to the star formation history and can be strongly affected by dust extinction (Cardelli et al. 1989; Fitzpatrick & Massa 2007). The near-infrared luminosity emitted by the old stellar population is fairly insensitive to dust extinction, and is thus considered as a reliable indicator of the total stellar mass of a galaxy (Bruzual & Charlot 2003; Maraston 2005). In our work, we restrict the distance to 400Mpc as it is reasonably above the limiting sensibility distance of LIGO-Virgo for binary neutron star merger with O3 sensibility (Chen et al. 2017). In the version 2.3 of the GLADE catalog, only ~67% of the galaxies up to 400Mpc have a K band magnitude. As showed by (Norris et al. 2014), the WISE1 (3.4 μm) luminosity is a reliable indicator of the stellar mass, and the AllWISE catalog (Cutri & et al. 2014) is all-sky. Therefore we perform a crossmatch with the AllWISE catalog to increase the number of galaxies with a near infrared magnitude to derive a reliable stellar mass estimation. From WISE1 luminosities, (Kettlety et al. 2018; Norris et al. 2014) showed that the stellar mass of galaxies can be estimated with a mass to light ratio: $\Upsilon_*^{3.4\mu\text{m}} \sim 0.60M_\odot/L_{\odot,3.4\mu\text{m}}$

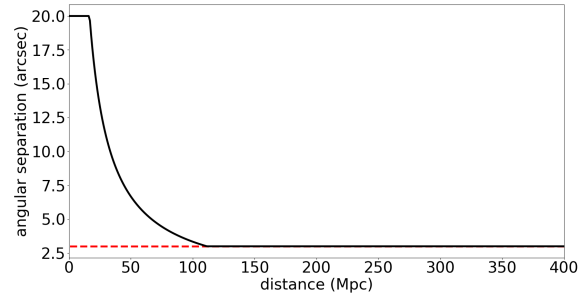


Figure 3. Angular separation condition used for the crossmatch as a function of the distance. The red dashed line show the limit value of 3 arcseconds.

where $M_\odot/L_{\odot,3.4\mu\text{m}}$ is the mass-to-light ratio in units of solar masses over the solar luminosity in the WISE 3.4 μm band ($m_{\odot,3.4\mu\text{m}} = 3.24\text{mag}$; $L_{\odot,3.4\mu\text{m}} = 1.58 \times 10^{32}\text{ergs}^{-1}$; (Jarrett et al. 2013)). This approach derives stellar mass with an error of 0.10 dex (Kettlety et al. 2018; Norris et al. 2014). Although the value of $\Upsilon_*^{3.4\mu\text{m}}$ can vary from ~0.5 to ~0.65 in the literature, this results on small changes on the derived stellar mass and will not affect the ranking of the galaxies as it is a constant ratio.

We spatially crossmatched the GLADE catalog cut to 400Mpc with the AllWISE catalog using a radius crossmatch varying with the distance as seen in Figure 3. The radius is defined as 5% the angular diameter of the milky way (0.0324 Mpc) and we impose a minimum and maximum of 3 and 20 arcseconds respectively. This strategy was chosen to optimize the match at low distance where galaxies can have very large angular size. A same AllWISE object can appear more than once, meaning that there is more than one GLADE galaxy around the given AllWISE object. For such case, knowing the angular resolution of the WISE telescope in the WISE1 band (6.1 arc seconds), we only kept the closest object if it is the only one in a radius of 6.1 arc seconds around the GLADE galaxy. The presence of an AGN implies a significant emission in the infrared and near-infrared (Ruiz et al. 2013; Burtscher et al. 2015; Sanders 1999), and thus biased our stellar mass estimation for such galaxies. We identify active galactic nucleus (AGN) from the resulting catalog using the mid-infrared color criterion $W1 - W2 \geq 0.8$ as used in (Stern et al. 2012; Assef et al. 2018). This corresponds to 3363 galaxies, that are still present in the catalog but without stellar mass estimation.

We use the elliptical aperture photometry flux from ALLWISE catalog whenever available for the source, otherwise the profile fitting photometry is used. This ensures that these fluxes should encompass each galaxy full radial extent. At the end we obtain the stellar mass information for 743780 objects, knowing that GLADE catalog cut to 400 Mpc have 800986 galaxies we have a ~ 93% of match efficiency.

Before the conversion of WISE1 magnitudes to stellar masses using the mass-to-light ratio provided by (Kettlety et al. 2018), we apply a K-correction to correct for the distance. We use 31 SED templates covering all known type of galaxies, from red elliptical to blue star-forming galaxies (Ilbert et al. 2009). We compute the K-correction both

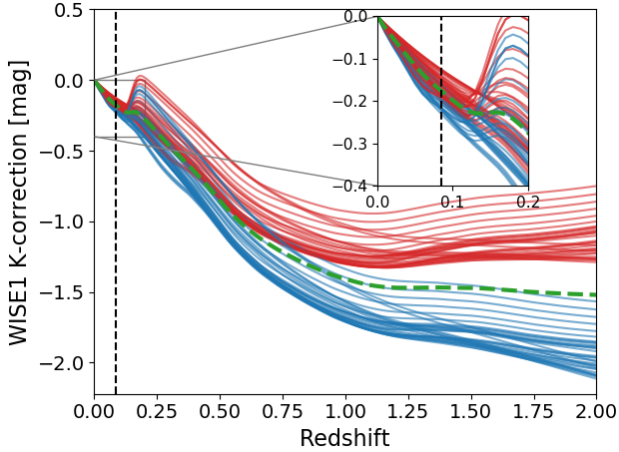


Figure 4. K-correction for the 31 galaxy SED templates for the redshift range 0 to 2 with a zoom-in from 0 to 0.2. The blue solid lines are for the SED templates without dust attenuation, red solid lines are with a dust attenuation of $E(B - V)=0.5$ mag using the Calzetti law (Calzetti et al. 2000). The green dashed line is the mean value at a given distance of the K-correction for all galaxies SED considered in this study. The black dashed line corresponds to 400Mpc.

without dust attenuation and with $E(B - V)=0.5$ mag using the Calzetti attenuation law (Calzetti et al. 2000). The K-correction is insensitive to the galaxy type and dust attenuation up to $z=0.12$ as seen in Figure 4. Given the distance limitation of 400Mpc ($z\sim 0.085$) for our catalog, we computed the K-correction at a given distance as the mean value for the 31 galaxies SED templates with and without dust attenuation. At this range of distances, the effect is negligible, however this will become important for future catalogs that will need to be deeper to encompass the sensitivity improvement of LIGO-Virgo interferometers.

3.2 Completeness of the Mangrove catalog

In this section, we aim at quantifying the completeness of the Mangrove catalog in terms of stellar mass. The stellar mass function is well described by a Schechter function (Schechter 1976), $\Phi(M)$, which parametrises the number density of galaxies, $n_{galaxies}$, as a function of their stellar mass. In this work, we use the low-redshift galaxy stellar mass function derived from the Galaxy And Mass Assembly (Wright et al. 2017), using a double Schechter function in logarithmic mass space defined as:

$$\begin{aligned}
 n_{galaxies} &= \Phi(M) d\log M \\
 &= \ln(10) e^{-10^{\log M - \log M^*}} \left[\Phi_1^* \cdot \left(10^{\log M - \log M^*}\right)^{\alpha_1 + 1} \right. \\
 &\quad \left. + \Phi_2^* \cdot \left(10^{\log M - \log M^*}\right)^{\alpha_2 + 1} \right] d\log M
 \end{aligned}
 \tag{7}$$

where $\log M^* = 10.78$, $\Phi_1^* = 2.93 \cdot 10^{-3} h^3 \text{Mpc}^{-3}$, $\Phi_2^* = 0.63 \cdot 10^{-3} h^3 \text{Mpc}^{-3}$, $\alpha_1 = -0.62$ and $\alpha_2 = -1.5$ (Wright et al. 2017).

Following the approach of (Gehrels et al. 2016; Dálya et al. 2018) regarding the luminosity function, we divided galaxies into 12 luminosity distance shells, with a width of 33.3 Mpc. For each shell, we construct histograms of WISE1 band derived stellar mass and integrate the double Schechter function for the same stellar mass bins in Figure 6. As the luminosity distance increases more and more low mass galaxies are missing. Regarding the double Schechter function derived from GAMA, the new catalog is fairly complete up to 33 Mpc in terms of stellar mass. In this work, we are interested in the more massive galaxies, so we computed the stellar mass, $M_{1/2}$, for which half of the stellar mass density is contributed by galaxies below and above this value. By computing $\int_{\log M_{1/2}}^{13} \log M \Phi(M) d\log M = 0.5 * \int_7^{13} \log M \Phi(M) d\log M$, we find $\log M_{1/2} = 10.674$. For all the luminosity distance shells, the Mangrove catalog distribution follows the double Schechter function for $\log M > \log M_{1/2}$ as seen in Figure 6. Our method is prioritising the more massive galaxies, consequently the fairly completeness relative to the double Schechter function for galaxies at $\log M > \log M_{1/2}$ minimises the lack of low mass galaxies as the distance increases.

4 VALIDATION ON GW170817 EVENT

At the time the event of the 17th august 2017 is the only gravitational wave event with a detected electromagnetic counterpart so our new method has to be tested on this event.

The GW170817 released distance is 40 ± 8 Mpc, the 90% sky map spans around 30deg^2 and as shown in the figure 2 according to our criteria (see Section 2 for the definition) there is 65 compatible galaxies within. The table in Appendix A shows the results for this event on the selection of galaxies and their ranking according to the standard approach (Equation 1), according to Arcavi et al. (2017), according to our method with product (Equation 3) and according to our method with addition (Equation 4). NGC 4993 host galaxy of GW170817 is ranked in 5th position in the standard approach. The (Arcavi et al. 2017) grade improved its rank to the 2nd position and is ranked first with our method for both (Equation 3) and (Equation 4) expressions. These results show that if we had used our grade to monitor this event, there would have been a gain in the speed of observation of the host galaxy. An important thing to see in those results is that the new grades are behaving like expected i.e. galaxies with high stellar mass are prioritized compared to galaxies with small stellar mass (see Appendix A where the list of galaxies for the four methods are reported with their grade and stellar mass if used). We also stress that galaxies with a high 3D probability but without stellar mass information also appear in the list (see Appendix A), for instance galaxy WINGSJ125701.38-172325.2 is ranked in 9th position, keeping such host candidate is a real improvement of the equation 4 compared to equation 3.

GW170817 was quite a lucky event in terms of distance of the source and good localisation thanks to data available for the three GW detectors. However, as the three interferometers are not always in operating mode, this is very common to have a two interferometers detection resulting

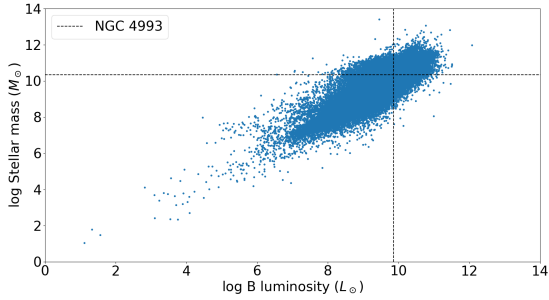


Figure 5. B band luminosity provided by GLADE as a function of the stellar mass determined with the constant mass to light ratio using the W1 band. The crossing of the dashed lines shows the NGC 4993 (host of GW170817) position on this plot.

in a poorer localisation (Abbott et al. 2018b). In order to test our method on a larger skymap, i.e. a two interferometers event, we choose to use the GW170817 skymap without Virgo data. The 90% skymap spans $\sim 190 \text{deg}^2$, this is a good example of two GW detectors localisation for which we can be sure of the counterpart host. According to our criteria in Section 2, there are 205 galaxies compatible with this skymap. The table in appendix B shows the resulting ranking for this skymap using the four presented grades. NGC 4993 host galaxy of the event is ranked in 27th position in the standard approach. The (Arcavi et al. 2017) grade ranks it at the 6th position and our grade is even more successful by putting NGC 4993 in the 4th position with both equations 3 and 4 expressions. Those results shows that the gain of our method for the follow up of gravitational waves event is even bigger in the case of wide skymap. This example of wider skymap allows us to see that sometime the (Arcavi et al. 2017) grade and our grades behave differently and even oppositely. For example the galaxy PGC043966 is ranked in 37th position with the standard grade and, when the Arcavi et al. (2017) grade upgrade its rank to the 30th, both of our grades (equations 3) and (4) downgrade its rank to the 54th and 49th position respectively. We can also note that the (Arcavi et al. 2017) grade ranked the NGC 4658 galaxy in first position due to its high B band luminosity but this galaxy is ranked in position 9 with our final grade definition. For these two examples the stellar mass estimation is not as high as the B band luminosity might suggest. Using the B band luminosity in those cases would have led to observe preferentially less massive galaxies. We illustrate the difference in the behavior between our grade and the one from (Arcavi et al. 2017) in Figure 5, where we plot the stellar mass estimation using WISE1 band as a function of the B band luminosity for the same galaxies. We see that for a given B band luminosity there is an important scatter in stellar mass spanning a few order of magnitudes. It means that the probability associated to a galaxy with respect to its stellar mass estimation can behave very differently for both methods. For example, for the host galaxy associated to GW170817, NGC 4993, we derived a stellar mass of $\sim 2.14 \times 10^{10} M_{\odot}$ but galaxies with similar B band luminosity ($\sim 10^{10} L_{\odot}$) in the catalog span a stellar mass range from $\sim 3.8 \times 10^7 M_{\odot}$ to $\sim 1.0 \times 10^{12} M_{\odot}$ which repre-

sents almost five order of magnitudes. In addition to this different behavior, we also illustrate the flexibility of the grade defined in equation 4 by noting that using the grade defined in equation 3 would have led to drop out $\sim 13\%$ of the galaxies inside the 400Mpc of Mangrove catalog, and $\sim 5\%$ of the galaxies when using the B band luminosity as in (Arcavi et al. 2017).

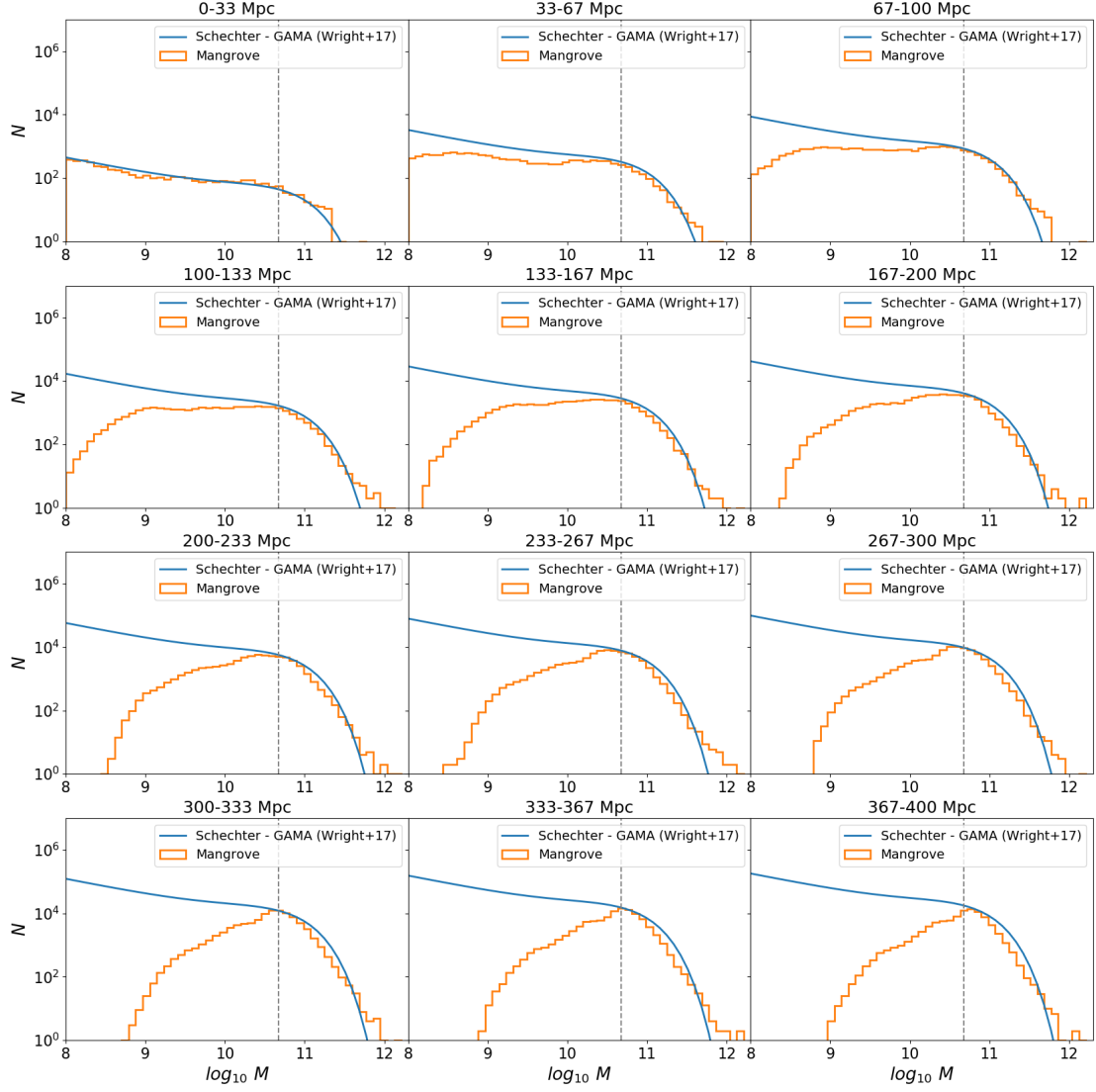


Figure 6. Stellar mass histograms for the Mangrove catalog at different luminosity distance shells compared to the double Schechter function derived from GAMA (Wright et al. 2017) weighted by the volume of each shell. Each panel is divided in 50 bins of $\log M$. The black dashed line represents the stellar mass, $\log M_{1/2}$ for which half of the stellar mass density is contributed by galaxies at $\log M > \log M_{1/2}$.

5 DISCUSSION AND CONCLUSION

5.1 Utilisation of the galaxies for the tiling

In this section we present a future development to use the galaxies for wide field of view telescopes. For the optimisation of wide FoV telescopes ($\gtrsim 1 \text{deg}^2$) follow up observations the standard approach consists in defining tiles over the sky and ranking them according to a given grade (Coughlin et al. 2018; Ghosh et al. 2016b). A first version of the grade of a tile you can build is:

$$Grade_{tile} = \sum_{pixel \in tile} P_{2D,pixel} \quad (8)$$

where we sum up the 2D probability of the pixels $P_{2D,pixel}$ within the tile. When using a catalog of galaxies one can define a "galaxy weighted" grade for the tile using the grade of the galaxies:

$$Grade_{tile} = \sum_{gal \in tile} Grade_{gal} \quad (9)$$

where we sum up the grade of the galaxies within the tile. In this expression any galaxy grade can be used, such as the expression in equation 4 that will optimise the chance to find the GW electromagnetic counterpart. The biggest issue of this approach is the catalog completeness, which makes this approach valid only below a distance threshold above which one has to switch back from grade definition of equation 9 to equation 8 in order to prevent using only galaxy information at a distance where your catalog is not complete enough.

We present a reformulation of the tile grade using our developments which allows to use galaxies catalog and a galaxy weighted grade at any distances. From Section 3.2, we are able to define the mass completeness of the catalog, $C_{m1,m2}^{d1,d2}$, between distances d_1 and d_2 for a stellar mass range between m_1 and m_2 comparing to the double Schechter function:

$$C_{m1,m2}^{d1,d2} = \int_{m1}^{m2} M_* f_{Schechter}(M_*) dM_* - \int_{m1}^{m2} M_* histogram(M_*) dM_* \quad (10)$$

With this parameter defining the completeness, we can define the grade of a given tile by:

$$P_{tile} = \sum_{pixel \in tile} \left[\sum_{gal \in pixel} P_{tot,gal} + (1 - C_{m1,m2}^{d1,d2}) P_{2D,pixel} \right] \quad (11)$$

where the first sum over all pixels inside the tile, the second sum over all galaxies falling in the 2D location of the pixel, $P_{tot,gal}$ is the grade of a given galaxy defined in Section 2.2, $P_{2D,pixel}$ is the 2D probability of the pixel, d_1 and d_2 are chosen as $\mu_{pixel} \mp \sigma_{pixel}$ respectively and m_1 and m_2 are fixed to 10^7 and 10^{13} (stellar mass range validity of the Schechter function fitted by Wright et al. (2017)). This expression removes any distance limitation for the use of galaxies weighted tiles. Note that with this expression we simply sum up the probability of the galaxies within a tile when the catalog is complete, whereas we sum up the 2D probability of all pixels within a tile when the catalog is not complete.

5.2 Conclusion

The electromagnetic follow-up of gravitational wave events is very challenging, the poor localisation of the source provided by LIGO-Virgo forces telescopes around the world to observe large areas of the sky. As the electromagnetic counterpart is expected to decay rapidly in luminosity, an optimisation is required to perform a rapid and efficient follow-up of the skymap. Recent developments in both catalog of galaxies and galaxy targeting strategy already optimised significantly the follow-up of such event. Our work provides an efficient tool to upgrade in one hand a catalog of galaxies by adding the stellar mass information and on the other hand the galaxy targeting approach with a new expression of the grade using this stellar mass information to select and rank the galaxies. We crossmatched the GLADE and AllWISE catalogs to retrieve the WISE1 band luminosity to determine the stellar mass of $\sim 87\%$ of the galaxies inside the GLADE catalog up to 400Mpc. This catalog is complete in terms of stellar mass up to $\sim 33\text{Mpc}$, and up to 200Mpc if we consider galaxies contributing to half of the stellar mass density. The new formulation of the grade presented in this work allows not only to use the 3D position of galaxies to select them but also their stellar mass. We tested and validated our grade on the GW170817 event by showing an improvement on the ranking of interesting galaxies, i.e. massive galaxies, where NGC4993 is ranked first. This work plainly encourages further developments of the galaxy targeting strategy including other physical properties of the galaxies, for instance by focusing low SFR galaxies, but such development are slowed down by the poor number of information available in the publicly available galaxy catalogs. The Mangrove catalog is publicly available at <https://mangrove.lal.in2p3.fr>, and this dedicated website automatically generates the list of galaxies, ranked by our new grade, compatible for each BNS event below 400Mpc, and observable from a given location on Earth. The improved grade presented in this work is implemented in the widely used *gwemopt*¹ python package (Coughlin et al. 2018), developed to optimize the efforts of electromagnetic follow-up of gravitational wave events.

ACKNOWLEDGEMENTS

We acknowledge the Virtual data of labex P2IO for the supply of IT resources. This work made use of the NASA/IPAC Extragalactic Database (NED).

REFERENCES

- Abbott B. P., et al., 2017a, *Phys. Rev. Lett.*, 119, 161101
 Abbott B. P., et al., 2017b, *ApJ*, 848, L13
 Abbott B. P., et al., 2018a, *Living Reviews in Relativity*, 21, 3
 Abbott B. P., et al., 2018b, *Living Reviews in Relativity*, 21, 3
 Abbott B. P., et al., 2018c, *Phys. Rev. Lett.*, 121, 161101
 Antolini E., Caiazzo I., Davé R., Heyl J. S., 2017, *MNRAS*, 466, 2212
 Arcavi I., et al., 2017, *ApJ*, 848, L33
 Artale M. C., Mapelli M., Giacobbo N., Sabha N. B., Spera M., Santoliquido F., Bressan A., 2019, *MNRAS*, 487, 1675

¹ <https://github.com/mcoughlin/gwemopt>

- Assef R. J., Stern D., Noirot G., Jun H. D., Cutri R. M., Eisenhardt P. R. M., 2018, *ApJS*, 234, 23
- Berger E., 2014, *ARA&A*, 52, 43
- Bruzual G., Charlot S., 2003, *MNRAS*, 344, 1000
- Burtscher L., et al., 2015, *A&A*, 578, A47
- Calzetti D., Armus L., Bohlin R. C., Kinney A. L., Koornneef J., Storchi-Bergmann T., 2000, *ApJ*, 533, 682
- Cardelli J. A., Clayton G. C., Mathis J. S., 1989, *ApJ*, 345, 245
- Chen H.-Y., Holz D. E., Miller J., Evans M., Vitale S., Creighton J., 2017, arXiv e-prints, p. [arXiv:1709.08079](https://arxiv.org/abs/1709.08079)
- Cook D. O., et al., 2019, *ApJ*, 880, 7
- Coughlin M. W., et al., 2018, *MNRAS*, 478, 692
- Coughlin M. W., Dietrich T., Heinzel J., Khetan N., Antier S., Christensen N., Coulter D. A., Foley R. J., 2019a, arXiv e-prints, p. [arXiv:1908.00889](https://arxiv.org/abs/1908.00889)
- Coughlin M. W., et al., 2019b, arXiv e-prints, p. [arXiv:1909.01244](https://arxiv.org/abs/1909.01244)
- Cutri R. M., et al. 2014, VizieR Online Data Catalog, p. II/328
- Dálya G., et al., 2018, *MNRAS*, 479, 2374
- Fitzpatrick E. L., Massa D., 2007, *ApJ*, 663, 320
- Gehrels N., Cannizzo J. K., Kanner J., Kasliwal M. M., Nissanke S., Singer L. P., 2016, *ApJ*, 820, 136
- Ghosh S., Bloemen S., Nelemans G., Groot P. J., Price L. R., 2016a, *A&A*, 592, A82
- Ghosh S., Bloemen S., Nelemans G., Groot P. J., Price L. R., 2016b, *A&A*, 592, A82
- Gill R., Nathanael A., Rezzolla L., 2019, *ApJ*, 876, 139
- Górski K. M., Hivon E., Banday A. J., Wand elt B. D., Hansen F. K., Reinecke M., Bartelmann M., 2005, *ApJ*, 622, 759
- Hajela A., et al., 2019, arXiv e-prints, p. [arXiv:1909.06393](https://arxiv.org/abs/1909.06393)
- Ilbert O., et al., 2009, *ApJ*, 690, 1236
- Im M., et al., 2017, *ApJ*, 849, L16
- Jarrett T. H., et al., 2013, *AJ*, 145, 6
- Kettlety T., et al., 2018, *MNRAS*, 473, 776
- Leibler C. N., Berger E., 2010, *ApJ*, 725, 1202
- Mapelli M., Giacobbo N., Toffano M., Ripamonti E., Bressan A., Spera M., Branchesi M., 2018, *MNRAS*, 481, 5324
- Maraston C., 2005, *MNRAS*, 362, 799
- Norris M. A., Meidt S., Van de Ven G., Schinnerer E., Groves B., Querejeta M., 2014, *ApJ*, 797, 55
- Rana J., Mooley K. P., 2019, arXiv e-prints, p. [arXiv:1904.07335](https://arxiv.org/abs/1904.07335)
- Ruiz A., Risaliti G., Nardini E., Panessa F., Carrera F. J., 2013, *A&A*, 549, A125
- Salafia O. S., Colpi M., Branchesi M., Chassande-Mottin E., Ghirlanda G., Ghisellini G., Vergani S. D., 2017, *ApJ*, 846, 62
- Sanders D. B., 1999, in Terzian Y., Khachikian E., Weedman D., eds, IAU Symposium Vol. 194, Activity in Galaxies and Related Phenomena. p. 25 ([arXiv:astro-ph/9903445](https://arxiv.org/abs/astro-ph/9903445))
- Schechter P., 1976, *ApJ*, 203, 297
- Singer L. P., Price L. R., 2016, *Phys. Rev. D*, 93, 024013
- Singer L. P., et al., 2016, *ApJ*, 829, L15
- Stern D., et al., 2012, *ApJ*, 753, 30
- Toffano M., Mapelli M., Giacobbo N., Artale M. C., Ghirlanda G., 2019, *MNRAS*, p. 2085
- Veitch J., et al., 2015, *Phys. Rev. D*, 91, 042003
- Wright A. H., et al., 2017, *MNRAS*, 470, 283
- Xie C., Fang T., Wang J., Liu T., Jiang X., 2016, *ApJ*, 824, L17

APPENDIX A:

Table A1: Ranking of the galaxies compatible with the GW170817 skymap according to grades defined in equations (1), (3) and (4), and the grade of (Arcavi et al. 2017).

Galaxy name	(1)		(Arcavi et al. 2017)		(3)		(4)		BLum (L_{\odot})	Stellar mass (M_{\odot})
	Rank	P_{loc}	Rank	P_{tot}	Rank	P_{tot}	Rank	P_{tot}		
ESO575-053	1	0.06	8	0.043	6	0.038	6	0.05	8.32e+35	9.675
PGC803966	2	0.059	35	0.003	35	0.001	8	0.033	5.96e+34	7.835
WINGSJ125701.38-172325.2	3	0.059	59	< 0.001	–	–	9	0.033	1.52e+33	–
ESO508-014	4	0.047	20	0.013	20	0.003	11	0.027	3.20e+35	8.605
NGC4993	5	0.046	2	0.111	1	0.22	1	0.123	2.79e+36	10.551
PGC797164	6	0.046	18	0.014	17	0.005	10	0.028	3.60e+35	8.864
ESO508-004	7	0.045	14	0.016	26	0.002	12	0.026	4.17e+35	8.416
IC4197	8	0.04	1	0.137	2	0.195	2	0.109	3.96e+36	10.563
ESO508-019	9	0.04	5	0.064	16	0.005	13	0.024	1.87e+36	9.004
2MASS 13104593-2351566	10	0.038	13	0.027	–	–	14	0.021	8.14e+35	–
796755	11	0.037	44	0.001	38	< 0.001	15	0.02	3.43e+34	7.9711
NGC4968	12	0.036	4	0.072	–	–	16	0.02	2.29e+36	–
6dFJ1309178-242256	13	0.034	33	0.003	36	0.001	17	0.019	1.05e+35	8.075
ESO508-010	14	0.033	11	0.04	7	0.036	7	0.035	1.39e+36	9.914
PGC169663	15	0.031	42	0.001	30	0.001	18	0.018	4.26e+34	8.171
IC4180	16	0.027	6	0.063	5	0.105	4	0.062	2.73e+36	10.466
PGC043966	17	0.024	15	0.016	29	0.001	20	0.014	7.77e+35	8.574
PGC799951	18	0.021	36	0.003	37	< 0.001	22	0.012	1.66e+35	8.247
WINGSJ125701.40-172325.3	19	0.021	–	–	–	–	23	0.011	–	–
ESO508-015	20	0.02	19	0.013	42	< 0.001	24	0.011	8.01e+35	7.885
ESO508-024	21	0.019	10	0.04	–	–	26	0.011	2.45e+36	–
ESO575-029	22	0.019	9	0.042	15	0.008	19	0.014	2.59e+36	9.49
PGC169670	23	0.017	40	0.002	31	0.001	28	0.01	1.05e+35	8.428
PGC772879	24	0.017	46	0.001	46	< 0.001	29	0.01	5.72e+34	7.862
NGC4970	25	0.017	3	0.081	3	0.139	3	0.071	5.54e+36	10.791
WINGSJ125701.40-172325.3	26	0.015	–	–	–	–	31	0.008	–	–
NGC4830	27	0.011	7	0.048	4	0.11	5	0.055	5.16e+36	10.882
PGC043664	28	0.01	16	0.015	14	0.01	27	0.01	1.71e+36	9.874
ESO575-061	29	0.01	37	0.002	43	< 0.001	34	0.006	2.74e+35	8.156
PGC044023	30	0.009	43	0.001	32	0.001	36	0.005	1.41e+35	8.693
PGC044312	31	0.008	39	0.002	23	0.002	37	0.005	2.86e+35	9.321
PGC044500	32	0.007	25	0.007	33	0.001	38	0.004	1.08e+36	8.787
PGC044021	33	0.006	26	0.006	28	0.001	39	0.004	1.16e+36	9.188
ESO508-033	34	0.006	24	0.007	12	0.012	30	0.009	1.29e+36	10.152
WINGSJ125217.42-153054.2	35	0.006	–	–	40	< 0.001	40	0.003	–	8.431
ABELL1644:[D80]141	36	0.005	–	–	–	–	42	0.003	–	–
ESO508-011	37	0.005	32	0.003	47	< 0.001	45	0.003	8.54e+35	8.302
PGC044478	38	0.004	29	0.004	45	< 0.001	46	0.002	1.08e+36	8.479
IC3799	39	0.004	12	0.028	11	0.012	33	0.008	8.50e+36	10.37
PGC183552	40	0.004	38	0.002	24	0.002	43	0.003	7.35e+35	9.568
ESO508-003	41	0.003	23	0.007	22	0.002	44	0.003	2.94e+36	9.754
NGC4763	42	0.003	17	0.015	9	0.02	25	0.011	6.15e+36	10.729
PGC044234	43	0.003	27	0.005	25	0.002	47	0.002	2.12e+36	9.679
ESO508-007	44	0.003	49	0.001	53	< 0.001	50	0.001	2.82e+35	7.609
PGC043908	45	0.003	30	0.004	18	0.003	41	0.003	1.68e+36	10.0
ESO575-035	46	0.002	34	0.003	39	< 0.001	51	0.001	1.66e+36	9.018
PGC043424	47	0.002	22	0.008	8	0.027	21	0.013	5.32e+36	11.051
IC3831	48	0.002	28	0.004	13	0.011	35	0.006	3.07e+36	10.698
PGC043505	49	0.002	55	< 0.001	44	< 0.001	53	0.001	1.66e+35	8.964
NGC4756	50	0.001	21	0.009	10	0.016	32	0.008	6.89e+36	10.904
PGC043344	51	0.001	47	0.001	–	–	54	0.001	5.20e+35	–
WINGSJ125252.62-152426.5	52	0.001	–	–	–	–	55	0.001	–	–
ESO508-020	53	0.001	48	0.001	–	–	58	0.001	5.69e+35	–
PGC910856	54	0.001	57	< 0.001	49	< 0.001	56	0.001	1.06e+35	8.75
PGC908166	55	0.001	56	< 0.001	48	< 0.001	57	0.001	1.71e+35	8.763
PGC043823	56	0.001	45	0.001	27	0.001	52	0.001	1.03e+36	9.937
PGC046026	57	0.001	41	0.001	21	0.002	49	0.002	1.72e+36	10.22
NGC4724	58	0.001	31	0.004	19	0.003	48	0.002	4.58e+36	10.365
PGC170205	59	0.001	50	0.001	–	–	60	< 0.001	1.01e+36	–

Continued on next page

Galaxy name	(1)		(Arcavi et al. 2017)		(3)		(4)		BLum (L_\odot)	Stellar mass (M_\odot)
	Rank	P_{loc}	Rank	P_{tot}	Rank	P_{tot}	Rank	P_{tot}		
PGC043913	60	0.001	51	< 0.001	34	0.001	59	0.001	9.78e+35	9.87
PGC937614	61	< 0.001	53	< 0.001	41	< 0.001	61	< 0.001	1.36e+36	9.79
PGC943386	62	< 0.001	58	< 0.001	51	< 0.001	62	< 0.001	4.77e+35	8.724
ESO575-041	63	< 0.001	54	< 0.001	50	< 0.001	63	< 0.001	1.20e+36	8.879
2MASS 12492243-1321162	64	< 0.001	52	< 0.001	–	–	64	< 0.001	2.01e+36	–
PGC942354	65	< 0.001	60	< 0.001	52	< 0.001	65	< 0.001	3.23e+35	8.723

APPENDIX B:

Table B1: Ranking of the galaxies compatible with the GW170817 without virgo data skymap according to grades defined in equations (1), (3) and (4), and the grade of (Arcavi et al. 2017).

Galaxy name	(1)		(Arcavi et al. 2017)		(3)		(4)		BLum (L_\odot)	Stellar mass (M_\odot)
	Rank	P_{loc}	Rank	P_{tot}	Rank	P_{tot}	Rank	P_{tot}		
ESO027-022	1	0.043	26	0.012	55	0.001	11	0.023	2.38e+35	7.958
ESO027-003	2	0.029	7	0.034	42	0.001	15	0.016	9.85e+35	8.461
NGC4348	3	0.028	2	0.058	1	0.145	1	0.083	1.73e+36	10.47
PGC1108616	4	0.027	88	0.001	80	< 0.001	16	0.014	1.81e+34	7.497
PGC3294456	5	0.027	101	< 0.001	92	< 0.001	17	0.014	1.14e+34	7.339
PGC3293647	6	0.025	112	< 0.001	64	< 0.001	19	0.013	7.33e+33	7.795
NGC4680	7	0.024	5	0.047	3	0.076	2	0.048	1.64e+36	10.252
1143004	8	0.024	100	< 0.001	–	–	20	0.013	1.41e+34	–
229961	9	0.021	47	0.004	46	0.001	21	0.012	1.54e+35	8.5336
NGC4663	10	0.019	14	0.025	10	0.046	6	0.032	1.13e+36	10.15
2MASS 22302645-7941381	11	0.018	32	0.009	63	< 0.001	24	0.01	4.27e+35	8.07
AGC229174	12	0.017	–	–	–	–	27	0.009	–	–
GAMA J121158.30+012934.6	13	0.016	–	–	102	< 0.001	29	0.008	–	7.416
NGC4658	14	0.015	1	0.102	8	0.047	8	0.03	5.59e+36	10.242
PGC069012	15	0.015	21	0.015	35	0.002	26	0.009	8.28e+35	8.885
ESO575-053	16	0.015	22	0.015	17	0.012	18	0.014	8.32e+35	9.675
UGC07184	17	0.015	24	0.014	47	0.001	30	0.008	8.07e+35	8.523
PGC803966	18	0.014	71	0.001	79	< 0.001	32	0.008	5.96e+34	7.835
PGC1183373	19	0.014	115	< 0.001	125	< 0.001	35	0.007	1.01e+34	6.987
WINGSJ125701.38-172325.2	20	0.014	155	< 0.001	–	–	36	0.007	1.52e+33	–
PGC797164	21	0.013	40	0.006	41	0.002	33	0.008	3.60e+35	8.864
SDSSJ121210.92+025255.6	22	0.013	108	< 0.001	93	< 0.001	38	0.007	1.64e+34	7.653
PGC1229057	23	0.013	83	0.001	70	< 0.001	39	0.007	4.22e+34	7.981
GAMA J122005.10+001556.4	24	0.012	–	–	86	< 0.001	40	0.007	–	7.715
PGC1066570	25	0.012	117	< 0.001	96	< 0.001	41	0.006	1.02e+34	7.65
ESO508-019	26	0.012	12	0.026	34	0.002	37	0.007	1.87e+36	9.004
NGC4993	27	0.012	6	0.038	4	0.071	4	0.04	2.79e+36	10.551
6dFJ1309178-242256	28	0.012	61	0.001	66	< 0.001	44	0.006	1.05e+35	8.075
ESO508-004	29	0.012	39	0.006	59	0.001	43	0.006	4.17e+35	8.416
ESO508-014	30	0.011	45	0.004	49	0.001	42	0.006	3.20e+35	8.605
PGC1060528	31	0.011	89	0.001	73	< 0.001	46	0.006	4.31e+34	8.025
PGC1193160	32	0.011	116	< 0.001	103	< 0.001	48	0.006	1.25e+34	7.563
IC4197	33	0.011	4	0.051	5	0.069	5	0.038	3.96e+36	10.563
796755	34	0.011	97	< 0.001	78	< 0.001	49	0.006	3.43e+34	7.9616
PGC3294393	35	0.011	119	< 0.001	82	< 0.001	51	0.006	1.16e+34	7.885
NGC4968	36	0.011	11	0.029	–	–	52	0.006	2.29e+36	–
PGC043966	37	0.01	30	0.01	54	0.001	47	0.006	7.77e+35	8.574
ESO027-001	38	0.01	3	0.056	2	0.084	3	0.045	4.61e+36	10.671
2MASS 00244271-7345157	39	0.01	27	0.011	38	0.002	45	0.006	9.43e+35	9.019
AGC229200	40	0.01	–	–	–	–	54	0.005	–	–
ESO027-008	41	0.01	8	0.033	6	0.054	7	0.031	2.85e+36	10.51
3091844	42	0.01	103	< 0.001	89	< 0.001	55	0.005	2.95e+34	7.7983
2MASS 13104593-2351566	43	0.009	31	0.009	–	–	56	0.005	8.14e+35	–
PGC3294258	44	0.009	129	< 0.001	123	< 0.001	57	0.005	8.62e+33	7.201
SDSSJ120404.33+044847.2	45	0.009	102	< 0.001	90	< 0.001	61	0.005	3.39e+34	7.834
PGC169663	46	0.009	98	< 0.001	69	< 0.001	60	0.005	4.26e+34	8.171
PGC1166504	47	0.009	113	< 0.001	99	< 0.001	62	0.005	2.05e+34	7.713
PGC772879	48	0.009	87	0.001	88	< 0.001	63	0.005	5.72e+34	7.862
UGC07185	49	0.009	79	0.001	114	< 0.001	64	0.005	7.50e+34	7.457

Continued on next page

Galaxy name	(1)		(Arcavi et al. 2017)		(3)		(4)		BLum (L_{\odot})	Stellar mass (M_{\odot})
	Rank	P_{loc}	Rank	P_{tot}	Rank	P_{tot}	Rank	P_{tot}		
ESO508-010	50	0.008	25	0.014	18	0.012	23	0.01	1.39e+36	9.914
ESO508-015	51	0.008	35	0.007	91	< 0.001	67	0.004	8.01e+35	7.885
IC4180	52	0.008	15	0.024	12	0.038	12	0.022	2.73e+36	10.466
NGC4123	53	0.008	16	0.02	19	0.01	28	0.009	2.18e+36	9.889
PGC3294218	54	0.007	136	< 0.001	116	< 0.001	70	0.004	9.35e+33	7.516
NGC4179	55	0.007	23	0.015	13	0.028	14	0.017	1.86e+36	10.377
PGC044021	56	0.006	33	0.009	40	0.002	66	0.004	1.16e+36	9.188
ESO027-021	57	0.006	28	0.01	20	0.01	31	0.008	1.41e+36	9.947
SDSSJ120736.32+024143.3	58	0.006	–	–	61	< 0.001	72	0.003	–	8.612
PGC1233241	59	0.006	154	< 0.001	130	< 0.001	74	0.003	3.92e+33	7.074
PGC799951	60	0.006	69	0.001	76	< 0.001	73	0.003	1.66e+35	8.247
PGC039902	61	0.005	52	0.003	81	< 0.001	75	0.003	4.15e+35	8.183
PGC037954	62	0.005	84	0.001	97	< 0.001	76	0.003	9.74e+34	7.971
ESO508-024	63	0.005	20	0.015	–	–	77	0.003	2.45e+36	–
PGC043664	64	0.005	29	0.01	25	0.007	50	0.006	1.71e+36	9.874
ESO575-029	65	0.005	19	0.015	32	0.003	68	0.004	2.59e+36	9.49
NGC5967	66	0.005	13	0.026	9	0.047	10	0.024	4.44e+36	10.739
J210518.19-824531.7	67	0.005	–	–	144	< 0.001	79	0.003	–	6.727
NGC4970	68	0.005	9	0.032	7	0.052	9	0.027	5.54e+36	10.791
UGC07332	69	0.005	68	0.001	134	< 0.001	80	0.003	2.12e+35	7.079
PGC2801913	70	0.005	–	–	27	0.005	59	0.005	–	9.819
NGC4116	71	0.005	38	0.006	33	0.002	71	0.003	1.14e+36	9.452
PGC169670	72	0.004	91	0.001	72	< 0.001	81	0.002	1.05e+35	8.428
SDSSJ121518.94+025538.2	73	0.004	145	< 0.001	129	< 0.001	82	0.002	7.72e+33	7.246
UGC07178	74	0.004	72	0.001	132	< 0.001	83	0.002	1.95e+35	7.171
WINGSJ125701.40-172325.3	75	0.004	–	–	–	–	85	0.002	–	–
NGC5967A	76	0.004	36	0.007	–	–	86	0.002	1.44e+36	–
UGC07396	77	0.004	42	0.005	67	< 0.001	84	0.002	1.11e+36	8.532
2MASS 15465869-7547149	78	0.004	49	0.003	–	–	87	0.002	6.51e+35	–
3293713	79	0.003	152	< 0.001	126	< 0.001	90	0.002	7.70e+33	7.506
ESO508-033	80	0.003	44	0.005	23	0.008	53	0.005	1.29e+36	10.152
IC3799	81	0.003	10	0.031	16	0.013	34	0.008	8.50e+36	10.37
3294175	82	0.003	164	< 0.001	153	< 0.001	93	0.002	2.11e+33	6.679
NGC4830	83	0.003	17	0.018	11	0.04	13	0.02	5.16e+36	10.882
GAMAJ121759.98+002558.1	84	0.003	–	–	154	< 0.001	94	0.002	–	6.522
WINGSJ125701.40-172325.3	85	0.003	–	–	–	–	95	0.002	–	–
PGC135791	86	0.003	123	< 0.001	142	< 0.001	98	0.001	3.90e+34	7.022
WINGSJ125217.42-153054.2	87	0.003	–	–	84	< 0.001	96	0.002	–	8.431
PGC043344	88	0.003	57	0.002	–	–	99	0.001	5.20e+35	–
PGC3271002	89	0.003	167	< 0.001	150	< 0.001	100	0.001	1.77e+33	6.814
ESO042-007	90	0.003	34	0.008	–	–	101	0.001	2.64e+36	–
SDSSJ114850.14+102655.9	91	0.003	–	–	101	< 0.001	103	0.001	–	8.229
NGC3976	92	0.002	18	0.018	15	0.018	25	0.01	5.96e+36	10.613
PGC037301	93	0.002	106	< 0.001	83	< 0.001	104	0.001	9.44e+34	8.488
ESO575-061	94	0.002	77	0.001	107	< 0.001	105	0.001	2.74e+35	8.156
PGC044023	95	0.002	99	< 0.001	71	< 0.001	102	0.001	1.41e+35	8.693
PGC3122921	96	0.002	165	< 0.001	152	< 0.001	107	0.001	2.58e+33	6.807
ESO508-035	97	0.002	105	< 0.001	117	< 0.001	108	0.001	1.01e+35	7.917
GAMAJ121732.70+002646.3	98	0.002	–	–	109	< 0.001	109	0.001	–	8.13
ESO068-002	99	0.002	67	0.001	105	< 0.001	110	0.001	4.94e+35	8.221
PGC044312	100	0.002	80	0.001	51	0.001	97	0.001	2.86e+35	9.321
PGC1070576	101	0.002	94	< 0.001	108	< 0.001	112	0.001	2.11e+35	8.248
6dFJ1258120-210246	102	0.002	95	< 0.001	95	< 0.001	114	0.001	2.18e+35	8.462
PGC044500	103	0.002	53	0.002	74	< 0.001	113	0.001	1.08e+36	8.787
SDSSJ115551.83+064354.9	104	0.002	135	< 0.001	122	< 0.001	118	0.001	3.90e+34	7.949
ESO508-007	105	0.002	92	0.001	131	< 0.001	120	0.001	2.82e+35	7.609
AGC215716	106	0.002	137	< 0.001	128	< 0.001	121	0.001	3.72e+34	7.743
PGC039799	107	0.002	118	< 0.001	151	< 0.001	123	0.001	7.89e+34	7.024
ABELL_1644:[D80]141	108	0.002	–	–	–	–	124	0.001	–	–
PGC037490	109	0.002	104	< 0.001	100	< 0.001	122	0.001	1.79e+35	8.473
HIPASSJ1255-15	110	0.001	–	–	–	–	127	0.001	–	–
ESO508-011	111	0.001	63	0.001	110	< 0.001	126	0.001	8.54e+35	8.302
PGC044478	112	0.001	59	0.002	106	< 0.001	129	0.001	1.08e+36	8.479
PGC183552	113	0.001	73	0.001	52	0.001	117	0.001	7.35e+35	9.568
PGC170205	114	0.001	65	0.001	–	–	132	0.001	1.01e+36	–

Continued on next page

Galaxy name	(1)		(Arcavi et al. 2017)		(3)		(4)		BLum (L_{\odot})	Stellar mass (M_{\odot})
	Rank	P_{loc}	Rank	P_{tot}	Rank	P_{tot}	Rank	P_{tot}		
IC3831	115	0.001	46	0.004	21	0.009	58	0.005	3.07e+36	10.698
PGC043424	116	0.001	37	0.007	14	0.02	22	0.01	5.32e+36	11.051
PGC1031551	117	0.001	163	< 0.001	159	< 0.001	134	< 0.001	7.36e+33	6.862
PGC3294523	118	0.001	172	< 0.001	164	< 0.001	136	< 0.001	1.86e+33	6.498
ESO508-003	119	0.001	51	0.003	50	0.001	125	0.001	2.94e+36	9.754
PGC720745	120	0.001	153	< 0.001	140	< 0.001	138	< 0.001	3.11e+34	7.62
IC0874	121	0.001	75	0.001	43	0.001	111	0.001	8.89e+35	10.016
PGC758254	122	0.001	156	< 0.001	146	< 0.001	139	< 0.001	2.69e+34	7.49
NGC4763	123	0.001	41	0.006	24	0.007	69	0.004	6.15e+36	10.729
PGC043908	124	0.001	60	0.001	45	0.001	116	0.001	1.68e+36	10.0
PGC3293619	125	0.001	180	< 0.001	162	< 0.001	141	< 0.001	6.67e+32	6.631
PGC046026	126	0.001	64	0.001	36	0.002	106	0.001	1.72e+36	10.22
NGC4724	127	0.001	48	0.004	31	0.003	92	0.002	4.58e+36	10.365
PGC685308	128	0.001	130	< 0.001	104	< 0.001	142	< 0.001	1.21e+35	8.765
PGC044234	129	0.001	58	0.002	57	0.001	131	0.001	2.12e+36	9.679
PGC091191	130	0.001	168	< 0.001	163	< 0.001	145	< 0.001	5.86e+33	6.666
NGC4756	131	0.001	43	0.005	22	0.008	65	0.004	6.89e+36	10.904
WINGSJ125252.62-152426.5	132	0.001	–	–	–	–	148	< 0.001	–	–
PGC3291384	133	0.001	179	< 0.001	170	< 0.001	149	< 0.001	8.83e+32	6.295
135794	134	0.001	174	< 0.001	166	< 0.001	150	< 0.001	2.31e+33	6.473
2MASXJ13242754-3025548	135	0.001	128	< 0.001	–	–	151	< 0.001	1.50e+35	–
PGC043505	136	0.001	125	< 0.001	98	< 0.001	147	< 0.001	1.66e+35	8.964
ESO575-035	137	0.001	70	0.001	94	< 0.001	146	< 0.001	1.66e+36	9.018
PGC043823	138	0.001	81	0.001	48	0.001	130	0.001	1.03e+36	9.937
NGC4504	139	0.001	86	0.001	68	< 0.001	140	< 0.001	9.58e+35	9.402
PGC3294233	140	0.001	178	< 0.001	–	–	152	< 0.001	9.60e+32	–
2MASXJ12490814-1124354	141	0.001	131	< 0.001	–	–	154	< 0.001	1.50e+35	–
PGC104686	142	0.001	148	< 0.001	–	–	155	< 0.001	5.98e+34	–
NGC5114	143	0.001	50	0.003	26	0.005	78	0.003	4.65e+36	10.774
ESO508-036	144	< 0.001	146	< 0.001	138	< 0.001	156	< 0.001	6.54e+34	7.924
PGC910856	145	< 0.001	139	< 0.001	111	< 0.001	153	< 0.001	1.06e+35	8.75
PGC041725	146	< 0.001	133	< 0.001	157	< 0.001	158	< 0.001	1.60e+35	7.166
NGC4487	147	< 0.001	85	0.001	65	< 0.001	144	< 0.001	1.14e+36	9.493
PGC908166	148	< 0.001	134	< 0.001	113	< 0.001	159	< 0.001	1.71e+35	8.763
PGC043913	149	< 0.001	96	< 0.001	58	0.001	135	< 0.001	9.78e+35	9.87
PGC3097711	150	< 0.001	181	< 0.001	173	< 0.001	161	< 0.001	1.14e+33	6.106
PGC141593	151	< 0.001	126	< 0.001	112	< 0.001	160	< 0.001	2.23e+35	8.8
PGC3097710	152	< 0.001	182	< 0.001	–	–	164	< 0.001	1.14e+33	–
PGC705472	153	< 0.001	144	< 0.001	156	< 0.001	163	< 0.001	9.78e+34	7.363
PGC937614	154	< 0.001	90	0.001	62	< 0.001	143	< 0.001	1.36e+36	9.79
ESO508-020	155	< 0.001	110	< 0.001	–	–	165	< 0.001	5.69e+35	–
NGC5061	156	< 0.001	54	0.002	29	0.004	89	0.002	4.95e+36	10.805
PGC135798	157	< 0.001	171	< 0.001	167	< 0.001	168	< 0.001	4.70e+33	6.665
PGC042120	158	< 0.001	173	< 0.001	169	< 0.001	169	< 0.001	3.98e+33	6.529
ESO444-026	159	< 0.001	56	0.002	–	–	170	< 0.001	4.64e+36	–
J132249.66-300651.8	160	< 0.001	–	–	119	< 0.001	166	< 0.001	–	8.706
PGC943386	161	< 0.001	114	< 0.001	118	< 0.001	167	< 0.001	4.77e+35	8.724
PGC3097712	162	< 0.001	177	< 0.001	174	< 0.001	172	< 0.001	1.80e+33	6.13
PGC3294387	163	< 0.001	184	< 0.001	172	< 0.001	171	< 0.001	4.59e+32	6.383
PGC3268622	164	< 0.001	183	< 0.001	160	< 0.001	173	< 0.001	5.02e+32	7.236
PGC3097709	165	< 0.001	176	< 0.001	171	< 0.001	174	< 0.001	2.38e+33	6.406
PGC046803	166	< 0.001	93	< 0.001	53	0.001	133	< 0.001	1.43e+36	10.154
PGC104868	167	< 0.001	158	< 0.001	148	< 0.001	175	< 0.001	4.53e+34	7.848
ESO444-021	168	< 0.001	66	0.001	87	< 0.001	162	< 0.001	4.08e+36	9.381
WINGSJ132507.84-315046.2	169	< 0.001	–	–	–	–	177	< 0.001	–	–
NGC5078	170	< 0.001	55	0.002	28	0.004	88	0.002	6.52e+36	10.978
ESO444-011	171	< 0.001	111	< 0.001	120	< 0.001	176	< 0.001	7.74e+35	8.824
ESO508-039	172	< 0.001	151	< 0.001	158	< 0.001	179	< 0.001	1.09e+35	7.434
NGC4748	173	< 0.001	82	0.001	37	0.002	115	0.001	2.32e+36	10.672
J132044.59-302043.7	174	< 0.001	–	–	–	–	181	< 0.001	–	–
ESO444-012	175	< 0.001	78	0.001	56	0.001	137	< 0.001	3.17e+36	10.26
PGC141595	176	< 0.001	141	< 0.001	121	< 0.001	180	< 0.001	2.06e+35	8.881
PGC850539	177	< 0.001	122	< 0.001	127	< 0.001	183	< 0.001	5.31e+35	8.668
PGC740755	178	< 0.001	132	< 0.001	–	–	184	< 0.001	3.76e+35	–
ESO444-002	179	< 0.001	157	< 0.001	161	< 0.001	186	< 0.001	1.03e+35	7.375

Continued on next page

Galaxy name	(1)		(Arcavi et al. 2017)		(3)		(4)		BLum (L_{\odot})	Stellar mass (M_{\odot})
	Rank	P_{loc}	Rank	P_{tot}	Rank	P_{tot}	Rank	P_{tot}		
PGC763675	180	< 0.001	159	< 0.001	155	< 0.001	187	< 0.001	6.22e+34	7.643
NGC5124	181	< 0.001	62	0.001	30	0.003	91	0.002	6.38e+36	11.025
ESO444-033	182	< 0.001	140	< 0.001	147	< 0.001	188	< 0.001	2.69e+35	8.095
WINGSJ132507.84-315046.2	183	< 0.001	–	–	–	–	189	< 0.001	–	–
WINGSJ132507.85-315046.2	184	< 0.001	175	< 0.001	–	–	190	< 0.001	6.71e+33	–
PGC141602	185	< 0.001	138	< 0.001	143	< 0.001	191	< 0.001	3.89e+35	8.239
NGC5048	186	< 0.001	74	0.001	44	0.001	128	0.001	5.21e+36	10.713
PGC732248	187	< 0.001	143	< 0.001	139	< 0.001	192	< 0.001	2.49e+35	8.403
SDSSJ120133.99+042759.3	188	< 0.001	160	< 0.001	137	< 0.001	194	< 0.001	7.38e+34	8.456
NGC5051	189	< 0.001	76	0.001	39	0.002	119	0.001	4.78e+36	10.85
PGC046903	190	< 0.001	150	< 0.001	–	–	195	< 0.001	1.95e+35	–
IC0879	191	< 0.001	147	< 0.001	115	< 0.001	193	< 0.001	2.54e+35	9.272
PGC141596	192	< 0.001	121	< 0.001	85	< 0.001	182	< 0.001	9.42e+35	9.764
PGC722221	193	< 0.001	170	< 0.001	168	< 0.001	198	< 0.001	2.70e+34	7.113
PGC117211	194	< 0.001	162	< 0.001	136	< 0.001	197	< 0.001	8.52e+34	8.687
ESO444-015	195	< 0.001	107	< 0.001	75	< 0.001	178	< 0.001	2.42e+36	10.053
HIPASSJ1457-67	196	< 0.001	–	–	133	< 0.001	196	< 0.001	–	8.823
PGC042964	197	< 0.001	166	< 0.001	165	< 0.001	199	< 0.001	6.01e+34	7.317
ESO575-041	198	< 0.001	127	< 0.001	135	< 0.001	200	< 0.001	1.20e+36	8.879
PGC939548	199	< 0.001	149	< 0.001	141	< 0.001	201	< 0.001	4.06e+35	8.62
PGC1295846	200	< 0.001	161	< 0.001	145	< 0.001	203	< 0.001	1.76e+35	8.642
PGC2793691	201	< 0.001	142	< 0.001	–	–	204	< 0.001	7.10e+35	–
ESO443-086	202	< 0.001	124	< 0.001	124	< 0.001	202	< 0.001	1.88e+36	9.436
PGC043964	203	< 0.001	120	< 0.001	77	< 0.001	185	< 0.001	2.56e+36	10.361
NGC5126	204	< 0.001	109	< 0.001	60	< 0.001	157	< 0.001	4.67e+36	10.816
PGC104887	205	< 0.001	169	< 0.001	149	< 0.001	205	< 0.001	8.69e+34	8.616